Aerosol optical properties observed during Campaign of Air Quality Research in Beijing 2006 (CAREBeijing-2006): Characteristic differences between the inflow and outflow of Beijing city air

R. M. Garland,[1] O. Schmid,[2] A. Nowak,[3] P. Achtert,[3] A. Wiedensohler,[3] S. S. Gunthe,[1] N. Takegawa,[4] K. Kita,[5] Y. Kondo,[4] M. Hu,[6] M. Shao,[6] L. M. Zeng,[6] T. Zhu,[6] M. O. Andreae,[1] and U. Pöschl[1]

Received 15 July 2008; revised 5 November 2008; accepted 19 November 2008; published 14 February 2009.

[1] Ground-based measurements of aerosol optical properties were conducted during Campaign of Air Quality Research in Beijing 2006 (CAREBeijing-2006) (11 August to 9 September 2006) at a suburban site ~30 km south of Beijing. Averaged over the measurement campaign (arithmetic mean ± standard deviation), the total scattering coefficients (σ_s) were 469 ± 374 Mm^{-1} (450 nm), 361 ± 295 Mm^{-1} (550 nm), and 249 ± 206 Mm^{-1} (700 nm) and the absorption coefficient (σ_a) was 51.8 ± 36.5 Mm^{-1} (532 nm). The average Ångström exponent was 1.42 ± 0.19 (450 nm/700 nm) and the average single scattering albedo (ω_{532}) was 0.86 ± 0.07 (532 nm) with minimum values as low as 0.5. Pronounced diurnal cycles were observed in σ_s, σ_a, and ω_{532} and can be explained by boundary layer mixing effects. Additionally, an enhancement of absorbing particles in the early morning (0500–0800 local time) was observed; this may be attributed to soot emissions from traffic activity. When the measured air masses originated in the north and passed over Beijing, the single scattering albedo was generally low ($\omega_{532} < 0.8$), which indicates that the local emissions of particulate matter in Beijing were dominated by primary particles from combustion sources (soot). The southerly inflow to Beijing had typically very high σ_s and higher than average ω_{532} values, suggesting a large amount of secondary aerosol (e.g., sulfate and oxidized organics). Overall, the results suggest that a majority of the particle pollution in Beijing is transported into the city from the south.

Citation: Garland, R. M., et al. (2009), Aerosol optical properties observed during Campaign of Air Quality Research in Beijing 2006 (CAREBeijing-2006): Characteristic differences between the inflow and outflow of Beijing city air, *J. Geophys. Res.*, *114*, D00G04, doi:10.1029/2008JD010780.

1. Introduction

[2] Beijing, the capital of China and the site of the 2008 Summer Olympics, is a megacity with a population of over 14 million people in northeastern China (eBeijing, Beijing Official Website, http://www.ebeijing.gov.cn/default.htm). The city is surrounded by the Yanshan Mountains from the west to the northeast and has heavily industrialized areas from the southwest to the east [*Chen et al.*, 2007; *Streets et al.*, 2007]. The population in Beijing has been growing by ~2% annually since 1990 and the urban area has expanded to accommodate this, both through increased construction as well as expansion into the suburbs (Figure 1) [*Chan and Yao*, 2008]. This increase in urbanization and population growth has had widespread negative impacts on the surrounding environment. For example, a national survey in 2004 found that 57% of the monitoring stations on the Haihe River, which provides Beijing with the bulk of its drinking water, had a higher level of pollutants than the nation's drinking water standards allow [*Shao et al.*, 2006]. Air pollution in China may be considered its largest environmental problem, with nearly 70% of urban areas not in compliance with the country's air quality standards [*Shao et al.*, 2006].

[3] Particulate matter, especially particles with diameters less than 10 μm, was the major air pollutant in Beijing ~90% of the time in 1999–2005 and contributed to a decrease in visibility to lower than 10 km for ~180 days annually in 1999–2004 (see Beijing Environmental Bulletin, Beijing Municipal Environmental Protection Bureau, 1994–2005) [see also *Chan and Yao*, 2008]. This pollution is not only due to the emissions in Beijing itself. Rather, when the winds come from the south and southeast and pass over highly industrialized areas to the south (i.e., Hebei

[1]Biogeochemistry Department, Max Planck Institute for Chemistry, Mainz, Germany.
[2]Institute for Inhalation Biology, German Research Center for Environmental Health, Helmholtz Center Munich, Neuherberg, Germany.
[3]Leibniz Institute for Tropospheric Research, Leipzig, Germany.
[4]RCAST, University of Tokyo, Tokyo, Japan.
[5]College of Science, Ibaraki University, Mito, Japan.
[6]State Key Joint Laboratory of Environmental Simulation and Pollution Control, College of Environmental Sciences and Engineering, Peking University, Beijing, China.

0148-0227/09/2008JD010780

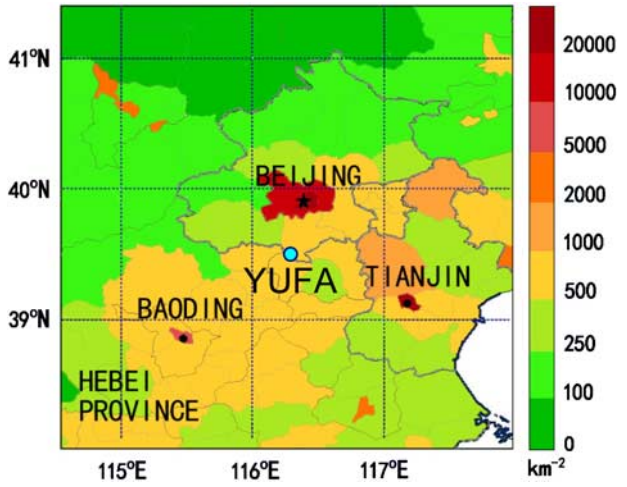

Figure 1. Suburban Yufa measurement site location (blue dot) along with surrounding area. The map is color-coded by population density (km^{-2}).

Province and Tianjin Municipality) the air quality in Beijing is greatly impacted [*Xia et al.*, 2007b]. Previous studies have found that particulate matter in the urban and surrounding areas follow similar trends in concentration and are at times spatially uniform, thus suggesting that the particulate pollution is regional in nature [*Chan and Yao*, 2008; *Xia et al.*, 2005].

[4] Models have suggested that the particulate pollution in Beijing originates from a combination of regional and local sources. These models have predicted that ~34% of PM2.5 [*Streets et al.*, 2007] and ~37.9% of PM10 [*Chen et al.*, 2007] in urban Beijing have regional sources. In both these studies, Hebei Province to the south (see Figure 1) was generally the largest contributor to the particulate pollution in Beijing, contributing up to 70% of both PM2.5 and PM10 in July 2001 and 2002, respectively [*Chen et al.*, 2007; *Streets et al.*, 2007]. Under the same conditions, Tianjin Municipality was the second largest contributor [*Chen et al.*, 2007; *Streets et al.*, 2007].

[5] Owing to the impact of regional sources, the aerosol concentration in Beijing is highly dependent upon air mass origin. Previous studies probing the ambient column aerosol optical depth have reported abrupt changes in the aerosol optical thickness (AOT) with changes in wind direction [*Li et al.*, 2007a, 2007b; *Xia et al.*, 2007b]. When Beijing is experiencing slow winds from the south, the AOT is generally greater than when the winds are fast and from the north [*Li et al.*, 2007a, 2007b; *Xia et al.*, 2007b; *Yan et al.*, 2008]. During the summer, when the winds are usually from the south, previous column measurements have found that the AOT is greatest and the ambient aerosols exhibit enhanced single scattering albedos and Ångström exponents, indicating "brighter" and smaller aerosols than during rest of the year [*Li et al.*, 2007a, 2007b; *Xia et al.*, 2007a, 2006]. A ground-based measurement of aerosol optical properties ~100 km north of Beijing found similar trends in the aerosol light extinction with a maximum in the summer and fall; however the single scattering albedo was at a minimum in the spring and summer, which may be due to local combustion emissions [*Yan et al.*, 2008]. The work of *Wehner et al.* [2008] found that the aerosol particle number and size distributions in Beijing from 2004 to 2006 were also similarly dependent upon the air mass origin, with lowest PM1 and PM10 mass concentrations when the air mass originated in the northeast. In the current study, ground-based measurements of aerosol optical properties were measured south of Beijing to probe the regional particulate pollution as well as its impact on urban Beijing.

[6] Owing to the continued regional problem with air pollution, as well as the fact that Beijing was preparing for the 2008 Summer Olympic Games, there has been a push to fully characterize this regional pollution in order to implement effective controls. Aerosol optical property measurements were thus made as part of CAREBeijing-2006 at a site south of Beijing to characterize the optical properties of this regional particulate pollution during the period when the Olympic Games would be held in 2008. Owing to its position, this site could measure this inflow to Beijing (as the winds predominantly came from the south during the measurement period) to probe the regional impact on the city's particulate pollution as well as the outflow from Beijing (when there was a change in the wind direction to northerly winds).

2. Experiment

2.1. Measurement Location and Supporting Data

[7] The measurements were made at a suburban site on the campus of Huang Pu Military College in Yufa (39.51467°N, 116.30533°E), which is located ~30 km south of Beijing (Figure 1) as part of CAREBeijing-2006 (11 August to 9 September 2006). The instruments were located on the top floor of a four-story school building with the sample inlets and a meteorological station mounted on the roof. The average ambient temperature for the campaign was 24.6 ± 4.4°C, the average ambient RH was 71.0 ± 18.3% and the average ambient pressure was 1005 ± 4 hPa. The winds were generally slow (average local wind speed 1.70 ± 1.38 m s^{-1}) and came mostly from the south (average local wind direction 172 ± 93°).

[8] The main aerosol inlet used in this study was equipped with a Rupprecht & Patashnick PM10 inlet that was optimized for isokinetic flow conditions with a cyclone for the size cutoff (flow rate 16.7 L min^{-1}). The sample flow passed through stainless steel tubing (1.9 cm, 5.1 m) and a diffusion dryer with silica gel/molecular sieve cartridges (alternating regeneration with dry pressurized air, regeneration cycles 15–50 min, average RH = 29 ± 5%). After drying, the sample flow was split into separate lines. One line was for the aerosol optical instruments (0.94 cm stainless steel, ~5 m, flow rate 6 L min^{-1}). Another line was for the aerosol sizing instruments (particle diameter $\leq$ 10 μm), namely a Twin Differential Mobility Particle Sizer (TDMPS, IfT) and an Aerodynamic Particle Sizer (APS, TSI 3321). The inlet, dryer and size distribution measurements were operated by the Leibniz Institute for Tropospheric Research (IfT). The present study focuses on the aerosol optical properties; a detailed discussion of the particle size distributions will be presented elsewhere (P. Achtert et al., Hygroscopic growth of tropospheric particle number size distributions over the North China Plain, manuscript in preparation, 2009).

Table 1. Average Aerosol Optical Parameters for the CAREBeijing-2006 Campaign and Effective Limits of Detection for the Measured Extensive Properties[a]

Parameter	Average	ELOD
$\sigma_{s,450}$ (Mm^{-1})	469 ± 374	7
$\sigma_{bs,450}$ (Mm^{-1})	44.9 ± 31.8	0.8
$\sigma_{s,550}$ (Mm^{-1})	361 ± 295	5
$\sigma_{bs,550}$ (Mm^{-1})	37.0 ± 26.4	0.6
$\sigma_{s,700}$ (Mm^{-1})	249 ± 206	4
$\sigma_{bs,700}$ (Mm^{-1})	33.2 ± 24.5	0.6
$\sigma_{a,532}$ (Mm^{-1})	51.8 ± 36.5	6.5
$\mathring{a}_s$(550/700)	1.51 ± 0.20	
$\mathring{a}_s$(450/700)	1.42 ± 0.19	
$\mathring{a}_s$(450/550)	1.31 ± 0.18	
b_{450}	0.105 ± 0.016	
b_{550}	0.112 ± 0.018	
b_{700}	0.142 ± 0.018	
ω_{532}	0.86 ± 0.07	

[a]Average is arithmetic mean ± standard deviation. ELOD denotes effective limits of detection.

[9] The NO_2 measurements were required for correction of the photoacoustic spectrometer data. The NO_x and NO_y measurements were performed using a separate inlet and sampling line, which will be described in detail elsewhere (TECO 42CTL; operated by University of Tokyo). The CO concentration was measured using a nondispersive infrared absorption instrument (Model 48, Thermo Environmental Instruments, USA; operated by University of Tokyo). The instrument was coupled with a Nafion dryer (Perma-Pure Inc. USA) to reduce the interference from water vapor [*Takegawa et al.*, 2006].

2.2. Optical Instrumentation and Extensive Optical Properties

[10] Total aerosol particle scattering coefficients ($\sigma_{s,\lambda}$) and hemispheric backscattering coefficients ($\sigma_{bs,\lambda}$) at three different wavelengths (λ = 450 nm, 550 nm, and 700 nm) were measured with an integrating nephelometer (Model 3563, TSI). The nephelometer was operated at 5 L min^{-1} with a 2-min averaging time. An auto zero, where particle-free air was sampled, was performed every 2 h. The nephelometer contains two temperature sensors, one relative humidity sensor and a pressure sensor. These sensors are used to report room temperature and the conditions in the measurement chamber. The relative humidity (RH) of the sample flow into the optical instruments was 28 ± 4%. Within this RH range, no systematic correlation between sample flow RH and measured optical parameters was observed, indicating that the variations of drying efficiency had no significant influence on the optical measurement results. For the campaign, the average sampling pressure and temperature as measured inside the nephelometer were 1002 ± 4 hPa and 25 ± 1°C, respectively. The campaign average for the nephelometer lamp power was 50.1 ± 1.3 W.

[11] The nephelometer was calibrated with filtered air and CO_2 gas as described in the instrument's manual. The calibration was performed at the beginning, middle and end of the campaign. On average, the calibration constants were within ±2.5% of each other. The total scattering and backscattering data were corrected for systematic biases due to angular truncation errors and a non-Lambertian light source using the Ångström exponents that were calculated as described in section 2.3.1 [*Anderson et al.*, 1996; *Anderson and Ogren*, 1998]. On average, the corrected values were within 18% of the measured values for the whole campaign. The measured scattering coefficients for this campaign were within 8% of modeled values as described in the work of Y. F. Cheng et al. (Influence of mixing state on aerosol light absorption during air mass aging processing at a polluted regional site near Beijing, submitted to *Journal of Geophysical Research*, 2008).

[12] The effective limit of detection (ELOD) under the current operating condition was determined for the nephelometer signals using their respective zero signals collected during the instrument's auto zeroing time. The instrument's software automatically subtracted these zero values from the measured signals and the ELOD was three times the standard deviation of the zero signals. The campaign average ELOD values can be seen in Table 1. Any value below the ELOD was discarded. In the end, 0.01% of the nephelometer data were discarded owing to ELOD reasons.

[13] The aerosol particle absorption coefficient at 532 nm ($\sigma_{a,532}$) was determined with a photoacoustic spectrometer (PAS; Desert Research Institute, Reno, Nevada), which provides highly sensitive absorption measurements without interference by scattering signals. The instrument has been described elsewhere in detail [*Arnott et al.*, 1999]. Briefly, a flow of aerosol (0.8 L min^{-1}) enters into an acoustic resonator and is illuminated by laser light (Nd:YAG, λ = 532 nm, 50 mW) that is modulated at the acoustic resonator frequency (1510 Hz). The light energy absorbed by the aerosol particles is rereleased as heat, producing a pressure wave that is detected by a microphone. The instrument was operated with an integration time of ~10 s and calibrated with gaseous NO_2 (~1000 ppm) [*Arnott et al.*, 2000; *Schmid et al.*, 2006]. The data were averaged for 2 min to match the timescale of the nephelometer. The instrument noise was measured on the same timescale as the signal. The overall accuracy of the PAS calibration in this study was within 10%, thus the overall accuracy of the measured PAS absorption coefficients are also ±10% [*Schnaiter*, 2005]. A zero measurement with filtered (Acro 50 Filters, Gelman), particle-free air was performed every 10–15 min for a period of ~1 min. The absorption coefficient that was measured during the zeroing periods was set as 0 Mm^{-1}, thereby accounting for absorption by NO_2 (and any other potential gaseous absorbers). If, however, the ambient NO_2 concentration changed during the 10- to 15-min sampling period following the zeroing period, the recorded aerosol particle absorption coefficients can be influenced by the changing background signal from NO_2. Thus, the photoacoustic measurement data have been corrected for ambient NO_2 concentration as described by *Schmid et al.* [2006], except for the period of 1–9 September 2006 when ambient NO_2 measurement data were not available. However, almost all of the NO_2 corrected data (99.6%) were within 10% of the uncorrected data. Thus the fluctuations in NO_2 were generally small and it is safe to assume that the uncorrected data for the period after 1 September 2006 are not affected by any substantial errors.

[14] The PAS data were averaged over 2 min and the quality of the data was assured by excluding high noise events (noise (N) $\geq$ 30 Mm^{-1}, e.g., owing to strong external vibrations) along with their corresponding data points, as

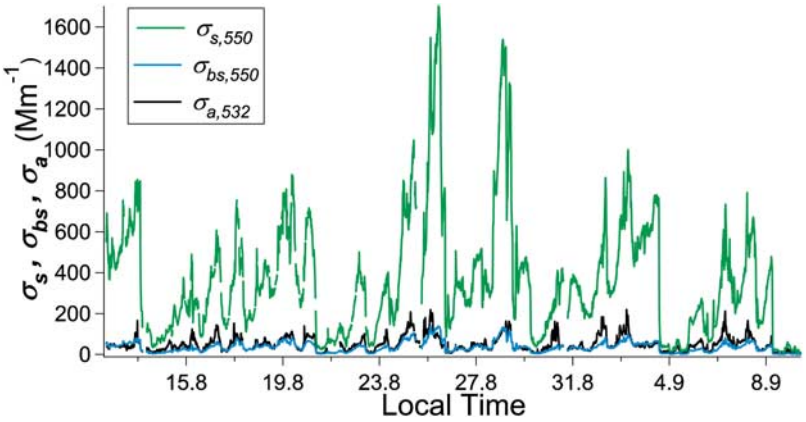

Figure 2. Time series for the extensive optical properties measured in the green spectral range: scattering, backscattering, and absorption coefficients ($\sigma_{s,550}$, $\sigma_{bs,550}$, and $\sigma_{a,532}$).

well as data below the effective limit of detection (ELOD). The $ELOD_{PAS}$ was defined as 3 times the average noise ($ELOD_{PAS} = 3 \sum_{i=1}^{n} N_i \, (n\sqrt{n})^{-1}$; N = 10-s noise data, n = number of points in 2-min averages; W. P. Arnott, personal communication, 2007). Any absorption coefficient data that were smaller than the ELOD for their respective time period were discarded (3.5% of data). The campaign average of the ELOD for the PAS (6.5 Mm^{-1}) was similar to the ELOD of the nephelometer (Table 1).

2.3. Intensive Properties

2.3.1. Ångström Exponent

[15] In analogy to aerosol optical depth or extinction, the wavelength dependence of aerosol scattering coefficients can be approximated by a power law [*Ångström*, 1929],

$$\sigma_{s,\lambda} = \sigma_{s,\lambda r} (\lambda/\lambda_r)^{-\mathring{a}_s}, \tag{1}$$

where $\sigma_{s,\lambda r}$ is the scattering coefficient at a given reference wavelength λ_r, and $\mathring{a}_s$ is the dimensionless Ångström exponent. The Ångström exponent corresponds to the slope of a double-logarithmic plot of σ_s versus λ and is calculated according to equation (2).

$$\mathring{a}_s(\lambda_1/\lambda_2) = -\frac{\log(\sigma_{s,\lambda_1}/\sigma_{s,\lambda_2})}{\log(\lambda_1/\lambda_2)}. \tag{2}$$

2.3.2. Backscattering Fraction and Single Scattering Albedo

[16] The angular corrected backscattering coefficient from the nephelometer is the scattered light intensity in the backward hemisphere of the particle (90°–180°) [*Anderson and Ogren*, 1998]. The hemispheric backscattering fraction, b_λ, is the ratio of this backscattering coefficient over the total scattering coefficient at a given wavelengths (λ = 450, 550, and 700 nm).

$$b_\lambda = \frac{\sigma_{bs,\lambda}}{\sigma_{s,\lambda}}. \tag{3}$$

[17] The single scattering albedo, ω_λ, is the ratio of the scattering coefficient over the extinction coefficient at a given wavelength. Here ω has been calculated at λ = 532 nm using equation (4).

$$\omega_{532} = \frac{\sigma_{s,532}}{\sigma_{s,532} + \sigma_{a,532}}. \tag{4}$$

The $\sigma_{s,532}$ was not measured directly by the nephelometer, but rather was calculated using equation (1) (λ_r = 550 nm), where $\mathring{a}_s$ was derived from equation (2) with the inputs, $\mathring{a}_s$ = $\mathring{a}_s$ (550/700) $\sigma_{s,\lambda 1} = \sigma_{s,550}$ and with λ_1 = 550 nm and λ_2 = 532 nm. Test calculations using $\mathring{a}_s$ (450/700) and $\mathring{a}_s$ (450/550) instead of $\mathring{a}_s$ (550/700) gave only slightly different results (relative deviations in $\sigma_{s,532}$ < 1%). Note that all reported extensive and intensive properties are for dry conditions (RH < 40%).

3. Results and Discussion

3.1. Overview of Optical Measurement Results (Time Series and Statistical Distribution)

3.1.1. Extensive Properties

[18] The time series for the aerosol particle total scattering ($\sigma_{s,550}$), backscattering ($\sigma_{bs,550}$) and absorption coefficients ($\sigma_{a,532}$) in the green spectral range for the entire campaign is displayed in Figure 2. The scattering and backscattering coefficients at λ = 450 nm and 700 nm ($\sigma_{s,450}$, $\sigma_{bs,450}$, $\sigma_{s,700}$, $\sigma_{bs,700}$) followed essentially the same trends as those for 550 nm.

[19] The extensive aerosol optical parameters displayed episodic behavior, with a buildup over several days followed by a "cleaning" where all measured parameters would decrease sharply. For example, on 3 September 2006 the $\sigma_{s,550}$ decreased by 94% from 765 Mm^{-1} at 1319 local time (LT) to 44.6 Mm^{-1} at 1539 LT and the $\sigma_{a,532}$ decreased by 76% (from 60 Mm^{-1} to 14 Mm^{-1}) in the same time period. Similar episodic behavior was observed in the aerosol mass loading and elemental carbon (EC) mass (i.e., higher mass loading and higher [EC] with southerly winds) as well as chemical composition; with southerly winds the particles were composed of a higher fraction of sulfate than the air masses from the north, which were dominated by organics (N. Takegawa et al., Variability of submicron aerosol observed at a rural site in Beijing in

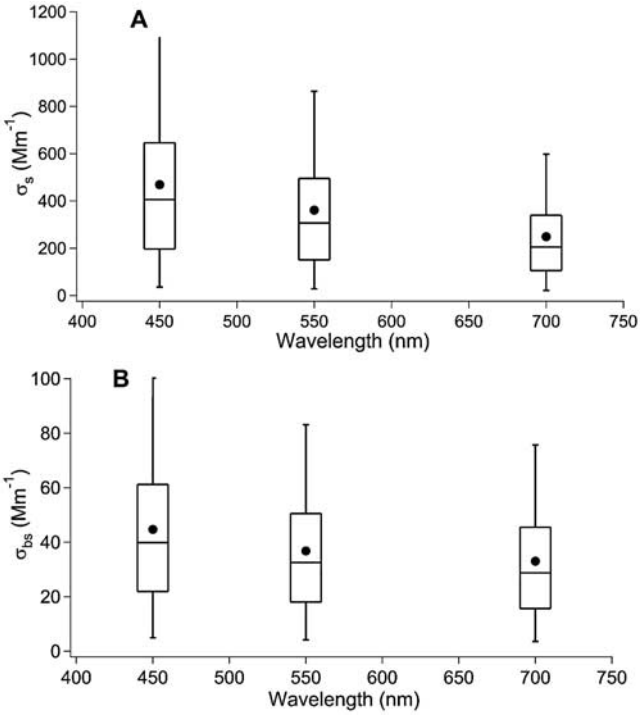

Figure 3. Statistical distribution of (a) scattering coefficients (σ_s) and (b) backscattering coefficients (σ_{bs}) measured with the three-wavelength nephelometer for the campaign. The dot is the mean value, the horizontal line in the box is the median, the limits of the boxes are the 25th percentile and 75th percentile, and the vertical lines extend to 5th and 95th percentiles.

the summer of 2006: Implications for regional processing, submitted to *Journal of Geophysical Research*, 2009).

[20] This abrupt change was due to a shift in wind direction from very slow local winds from the south to fast moving air masses from the northwest. In general all of these ''cleaning'' events were characterized by a change in the origin of the air mass from the south/southeast to the north. This will be discussed in more detail in section 3.3. The 20 highest $\sigma_{s,550}$ values of 1548–1703 Mm^{-1} were measured on 25 August 2006 in the late morning. The highest $\sigma_{a,532}$ value of 220 Mm^{-1} was measured on 2 September 2006 in the morning and the second highest value of 219 Mm^{-1} was measured on 25 August 2006 in the morning.

[21] The campaign arithmetic mean and standard deviation for the measured extensive properties are listed in Table 1, and the strong fluctuations described above are reflected by the high relative standard deviations (70–83%). Figure 3 summarizes the statistical distribution of the nephelometer data for the whole campaign. The mean and median values are represented by the dot and line in the box, respectively, and the top and bottom of the box are the 75th and 25th percentiles, respectively. The error bars indicate the 95th and 5th percentile. All similar statistical box plots shown in this paper will have the same structure. The mean values of the σ_s and σ_{bs} coefficients are generally well above the median value. For example, the median value for $\sigma_{s,550}$ is 307 Mm^{-1} while the mean value is 361 Mm^{-1}, which is 18% larger than the median value. This difference indicates a non-Gaussian distribution of the data with some very large values (i.e., during pollution episodes).

[22] The campaign averages of $\sigma_{s,550} = 361 \pm 295$ Mm^{-1} and $\sigma_{a,532} = 51.8 \pm 36.5$ Mm^{-1} are smaller than many reported values from previous studies in Beijing and the surrounding areas. *Bergin et al.* [2001] reported $\sigma_{s,530} = 488 \pm 370$ Mm^{-1} and $\sigma_{a,565} = 83 \pm 40$ Mm^{-1} from a 1-week intensive campaign in June 1999 on the campus of Peking University (in the northwest of Beijing). *Li et al.* [2007a] reported $\sigma_{s,550} = 468 \pm 472$ Mm^{-1} and $\sigma_{a,550} = 65 \pm 75$ Mm^{-1} from measurements in March 2005 at Xianghe (~70 km southeast of Beijing). The extensive properties are also smaller than those reported from urban Guangzhou ($\sigma_{s,545} = 463 \pm 178$ Mm^{-1} and $\sigma_{a,532} = 92 \pm 62$ Mm^{-1}) [*Andreae et al.*, 2008], but are similar to those from a study in the Yangtze delta ($\sigma_{s,530} = 353 \pm 202$ Mm^{-1} and $\sigma_{a,565} = 23 \pm 14$ Mm^{-1}) [*Xu et al.*, 2002] as well as a study southeast of Guangzhou in Xinken ($\sigma_{s,550} = 333 \pm 138$ Mm^{-1} and $\sigma_{a,550} = 70 \pm 42$ Mm^{-1}) [*Cheng et al.*, 2009]. The current study's results are larger than a study ~100 km northeast of Beijing ($\sigma_{s,525} = 174.6 \pm 189.1$ Mm^{-1}) [*Yan et al.*, 2008] as well as a study ~60 km northwest of Guangzhou ($\sigma_{s,550} = 151 \pm 103$ Mm^{-1} and $\sigma_{a,532} = 34.3 \pm 26.5$ Mm^{-1}) [*Garland et al.*, 2008]. An overview of scattering and absorption coefficients observed in other studies with comparable instrumentation and measurement conditions is given by *Garland et al.* [2008]. Overall, the average absorption and scattering coefficients observed in this study were higher than reported from other suburban areas but lower than those typically measured in the urban areas of Chinese megacities.

3.1.2. Intensive Properties

[23] The time series for the intensive optical parameters, the Ångström exponent ($\mathring{a}_s$), backscattering fraction (b), and single scattering albedo (ω_{532}), are displayed in Figure 4. Most of the abrupt changes in the extensive properties can also be seen in the intensive properties. Generally, as the extensive parameters sharply decreased, the ω_{532} and Ångström exponents decreased and the backscattering fraction increased. This will be discussed in more detail in section 3.3.

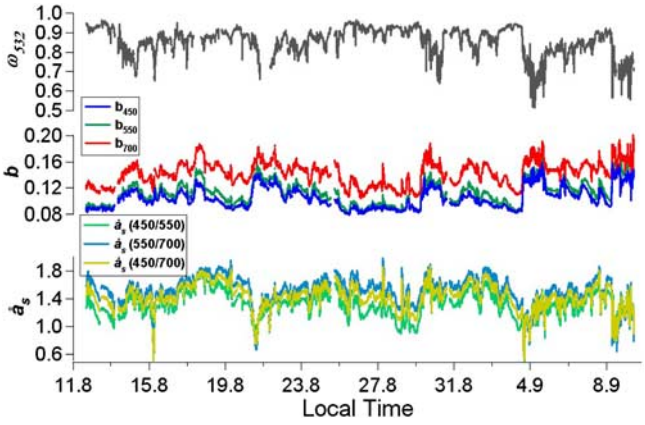

Figure 4. Time series for the intensive optical properties calculated for different wavelengths and wavelength pairs, respectively: single scattering albedo (ω_{532}), backscattering fraction (b), and Ångström exponent ($\mathring{a}_s$).

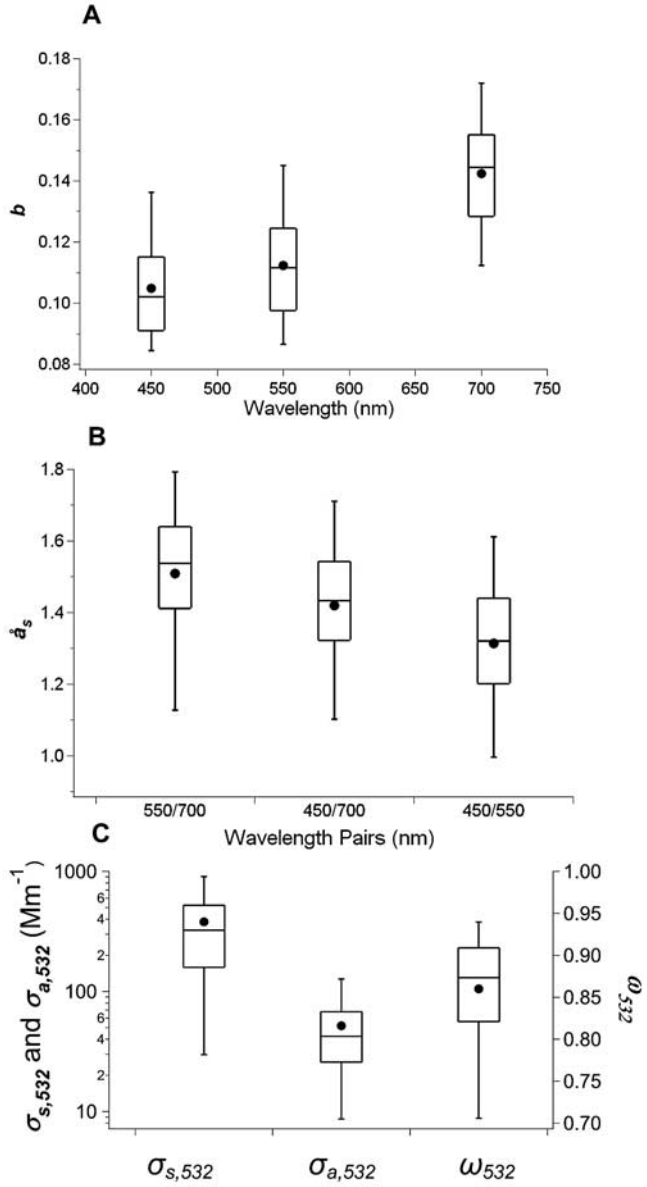

Figure 5. Statistical distribution of (a) backscattering fraction (b) for different wavelengths, (b) Ångström exponent ($\mathring{a}_s$) for different wavelength pairs, and (c) scattering and absorption coefficient and single scattering albedo at 532 nm ($\sigma_{s,532}$, $\sigma_{a,532}$, and ω_{532}) for the campaign. Symbols are analogous to Figure 3.

[24] Figure 5 displays box plots for the campaign statistics of b, $\mathring{a}_s$, $\sigma_{s,532}$, $\sigma_{a,532}$ and ω_{532}. The mean values and standard deviations of b were 0.105 ± 0.016 (450 nm), 0.112 ± 0.018 (550 nm), and 0.142 ± 0.018 (700 nm); and for $\mathring{a}_s$ were 1.51 ± 0.20 ($\mathring{a}_s$ (550/700)), 1.42 ± 0.19 ($\mathring{a}_s$ (450/700)) and 1.31 ± 0.18 ($\mathring{a}_s$ (450/550)). As seen in Figures 5a and 5b, both b and $\mathring{a}_s$ were dependent on wavelength. While b increased with increasing wavelength owing to decreasing size parameters, $\mathring{a}_s$ increased for the longer wavelength pairs owing to curvature in the log (σ_{sp}/Mm^{-1}) versus log (λ/nm) plot [*Garland et al.*, 2008].

[25] In Figure 5c, the interpolated $\sigma_{s,532}$ and measured $\sigma_{a,532}$ values are displayed. These two coefficients were used to calculate ω_{532}, which is also shown in Figure 5c. The mean and standard deviation of $\sigma_{s,532}$ for the campaign was 380 ± 309 Mm^{-1}, slightly larger than the measured $\sigma_{s,550}$. The mean and standard deviation for ω_{532} for the campaign was 0.86 ± 0.07, which is close to the values reported from other locations in and around Beijing and Guangzhou for the single scattering albedo of dry aerosol particles in the green spectral range (ω = 0.82–0.85 [*Andreae et al.*, 2008; *Bergin et al.*, 2001; *Cheng et al.*, 2009; *Garland et al.*, 2008; *Li et al.*, 1993]), indicating a smaller proportion of absorbing particulate matter at this suburban site. On the other hand, the Yufa average was lower than values reported for the Yangtze delta (ω = 0.93 ± 0.04 [*Xu et al.*, 2002]) and similar for a site ~100 km northeast of Beijing (ω = 0.88 [*Yan et al.*, 2008]).

[26] The relative standard deviations of the intensive parameters b, $\mathring{a}_s$ and ω_{532} (≤16%) were much smaller than those of the extensive parameters (σ_s and σ_a) and the statistical distributions were more symmetric; that is, the mean and median values were similar (within 3%). This indicates that changes in the intrinsic properties of the particles had less influence on the variation of extensive aerosol optical properties than changes in particle concentration.

3.2. Diurnal Cycles

[27] Figure 6 illustrates the diurnal cycles observed for the normalized extensive properties $\sigma_{s,550}$ and $\sigma_{a,532}$ as well as for the intensive properties ω_{532} and $\mathring{a}_s$ (450/700). In order to normalize the extensive properties data, each 2-min averaged data point was divided by its respective daily average; accordingly a value of 1 represents the daily average. The diurnal cycles of both extensive properties were characterized by near-constant values during the night and a minimum around midafternoon (1400–1600 LT). This diurnal pattern is consistent with the formation of a stable nocturnal boundary layer with continued local emissions in the evening, followed by a gradual breakup of this layer in the morning hours. This breakup is due to increasing convective activity in the boundary layer, which leads to mixing and dilution of the nocturnal boundary layer with air masses from the residual layer at higher altitudes.

[28] In addition to dilution effects, the $\sigma_{a,532}$ diurnal cycle appears to be also influenced by enhanced local emission sources of absorbing aerosol particles in the morning (~0500–0800 LT) when the cycle has its maximum. A similar enhancement is not seen in $\sigma_{s,550}$. Additionally, the diurnal cycle of ω_{532} displayed in Figure 6c resembles the diurnal cycle for the $\sigma_{a,532}$ as its mirror image with a maximum value of 0.88 in the afternoon (1100–1400 LT) and minimum of 0.82 at 0600 LT which coincides with the maximum in the $\sigma_{a,532}$ diurnal cycle. This decrease in ω_{532} in the morning along with no such peak in the $\sigma_{s,550}$ diurnal cycle, indicates that the morning peak in the $\sigma_{a,532}$ cycle is due to an increase in emission or accumulation of absorbing particles specifically.

[29] As shown in Figure 7, the diurnal cycles of [NO_y] and [CO] also peaked during the same time in the morning (0500–0800 LT) as $\sigma_{a,532}$ and ω_{532}, which suggests that the observed enhancement of absorbing particles was due to an increase in the local combustion emissions. This is consistent with the findings of Takegawa et al. (submitted

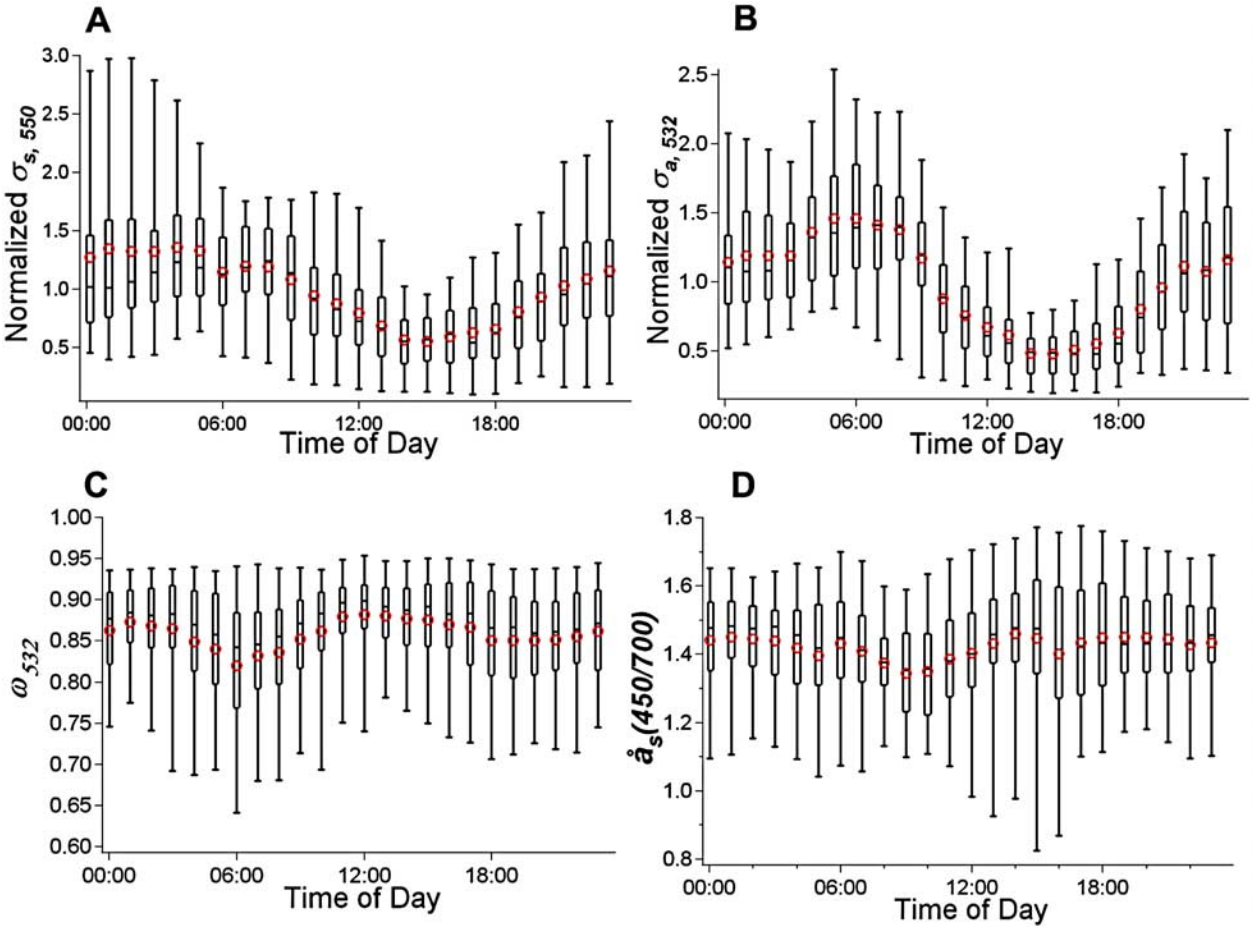

Figure 6. Diurnal cycles of normalized scattering and absorption coefficients, single scattering albedo and Angstrom exponent averaged over the campaign: (a) normalized $\sigma_{s,550}$, (b) normalized $\sigma_{a,532}$, (c) ω_{532}, and (d) $\mathring{a}_s$ (450/700).The dot is the mean value, the horizontal line in the box is the median, the limits of the boxes are the 25th percentile and 75th percentile, and the vertical lines extend to 5th and 95th percentiles for each 1-h period after the indicated start time.

manuscript, 2009), who inferred a morning peak of local diesel emissions from aerosol mass spectrometer composition and size data together with gas-phase data. The Ångström exponent exhibited a diurnal minimum at ~0900 LT. This decrease of $\mathring{a}_s$ (450/700) suggests an increase in the average particle diameter and may be due to resuspension of road dust, which is a major contributor to the coarse particle fraction in Beijing [*Wehner et al.*, 2008].

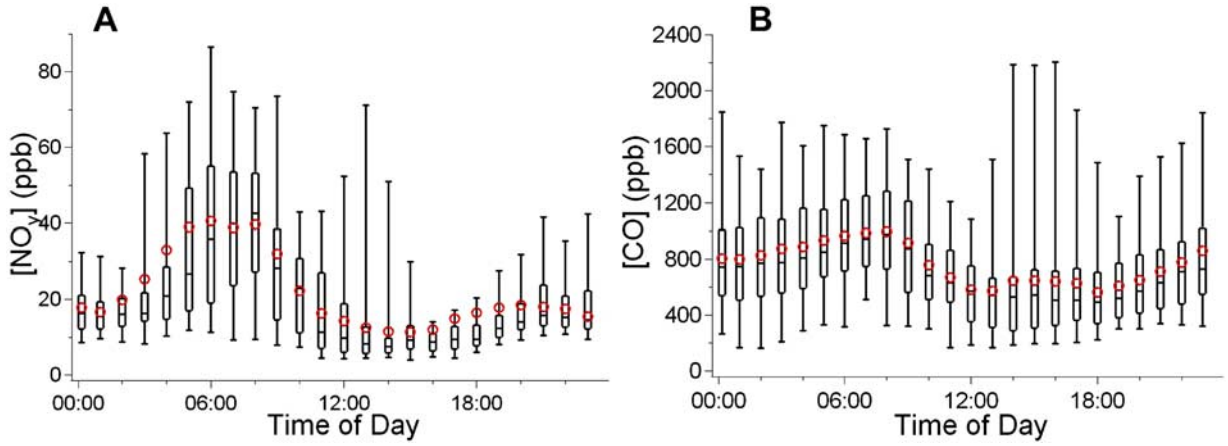

Figure 7. Diurnal cycles of the volume mixing ratios of (a) total reactive nitrogen, $[NO_y]$, and (b) carbon monoxide, [CO], averaged over the campaign. Symbols are analogous to Figure 6.

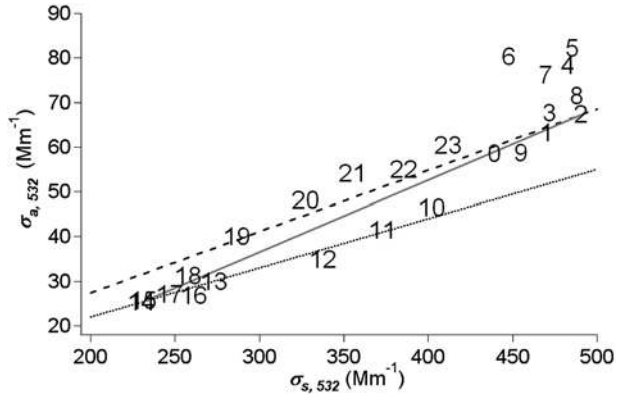

Figure 8. Mixing diagram for $\sigma_{a,532}$ and $\sigma_{s,532}$ relationship Characteristic "day values" at 1400 LT and "night values" at 0200 LT. The dotted and dashed lines are fit through each of these points and zero; the solid gray line represents linear mixing of "day" and "night" values. Data points are arithmetic mean values averaged over the campaign for 1-h periods after the indicated start time.

[30] The enhancement of absorbing particle emissions in the early morning can also be seen in a mixing plot as shown in Figure 8 [*Garland et al.*, 2008; *Keeling et al.*, 1996]. The hourly mean $\sigma_{a,532}$ and $\sigma_{s,532}$ values (points are labeled as "time of day") are displayed, along with a characteristic "night" value (0200 LT) and a characteristic "day" value (1400 LT). These two values are assumed to be generally representative of the $\sigma_{a,532}$ and $\sigma_{s,532}$ ratio (which is related to ω_{532}) seen during the night and day. If only "night" type aerosols were present, then the convective mixing that occurs upon the breakup of the nocturnal boundary layer in the morning would only dilute these aerosols and all points in Figure 8 would fall on the upper dashed line which is a linear fit between the "night" point and the graph's origin. However, if the diurnal cycles are strongly influenced by the formation and breakup of a nocturnal boundary layer, and the mixing that then occurs as described above, then this mixing will lead to a linear combination of lower ω_{532} "night" (particles representative of the nocturnal boundary layer) and higher ω_{532} "day" values.

[31] Since the aerosols present in the residual layer and the nocturnal layer have different ω_{532}, in the plot of $\sigma_{a,532}$ versus $\sigma_{s,550}$, the hourly mean values should move from a daytime value, reflecting the BL average ω_{532}, along a line (solid gray line in Figure 8) with a slope defined by the ω_{532} of the fresh emissions, toward a set of points that represent the composition of the aerosol in the nocturnal BL. The residual layer would continue to contain the more highly aged daytime particles with a higher ω_{532}. When convective mixing begins after sunrise, these two types of aerosols would mix, and the ω_{532} values measured through the morning would be a linear combination of the "night" aerosol particles with a low ω_{532} and the "day" aerosol particles with a high ω_{532}. Deviations from a straight mixing line indicate the addition (or removal) of aerosol components with a different ω_{532}, i.e., changes in primary emissions, secondary formation or atmospheric aging of particles.

[32] For most of the data points in Figure 8 the relative deviations from this simple conceptual model (represented by the solid gray line) are less than 10–20%. However, the early morning values (0400–0800 LT) are well above both the mixing line and the upper line representing average nighttime aerosol properties, which indicates increased absorption values during this time that cannot be ascribed to mixing. Thus, Figure 8 supports the idea that the diurnal cycles for the extensive properties and ω_{532} are generally controlled by the mixing of residual layer and nocturnal boundary layer with an enhancement of absorbing aerosols in the early morning that may be due to local traffic sources.

3.3. Back-Trajectory Analysis

[33] The time series of the extensive aerosol optical properties repeatedly showed an increase over several days followed by a sharp and sudden decrease (Figure 2). In general, these transitions were caused by a marked shift in prevailing wind direction, with the southerly winds leading to higher scattering and absorption coefficients. In order to probe these transitions, as well as the connection between air mass origin and aerosol optical properties, a few periods were highlighted (Table 2 and Figure 9). Back trajectories were calculated with the NOAA HYSPLIT model (R. R. Draxler and G. D. Rolph, HYSPLIT (HYbrid Single-Particle Lagrangian Integrated Trajectory) model, 2003, available at http://www.arl.noaa.gov/ready/hysplit4.html) using FNL meteorological data (B. Stunder, FNL inputs, 1997, available at http://www.arl.noaa.gov/ready-bin/fnl.pl) with a starting elevation of 100 m.

[34] Figure 9a displays the 24-h back trajectories for the highlighted days. Using these trajectories together with Table 2, it can be seen that there are large differences between the aerosol optical properties when the air mass came from the south within the previous 24 h (e.g., Periods 1–4) versus when the air mass recently came from

Table 2. Extensive and Intensive Aerosol Optical Properties for the Days Highlighted in Figure 9[a]

Period	Date	24-h Back Trajectory	$\sigma_{s,550}$ (Mm^{-1})	$\sigma_{a,532}$ (Mm^{-1})	$\hat{a}_s$(450/700)	b_{550}	ω_{532}
1	12 Aug 0000–2359 LT	S/SW	589 ± 111	47 ± 20	1.37 ± 0.07	0.091 ± 0.002	0.93 ± 0.02
2	18 Aug 0000–2359 LT	slow, S	408 ± 116	55 ± 15	1.69 ± 0.05	0.112 ± 0.004	0.89 ± 0.01
3	17 Aug 0000–2359 LT	S/SE	337 ± 185	65 ± 23	1.67 ± 0.09	0.127 ± 0.015	0.87 ± 0.02
4	31 Aug 0000–2359 LT	local, S	268 ± 65	38 ± 15	1.55 ± 0.10	0.113 ± 0.010	0.88 ± 0.03
5	20 Aug 0000–2359 LT	N/NE	227 ± 273	52 ± 41	1.02 ± 0.47	0.123 ± 0.020	0.72 ± 0.27
6	13 Aug 1400 LT to 14 Aug 1400 LT	NE	101 ± 52	30 ± 15	1.42 ± 0.11	0.119 ± 0.006	0.78 ± 0.05
7	3 Sept 1500 LT to 4 Sept 1500 LT	fast NW	35 ± 16	17 ± 9	1.11 ± 0.26	0.142 ± 0.006	0.68 ± 0.11
8	8 Sept 1000 LT to 9 Sept 1000 LT	fast NW	22 ± 15	12 ± 6	1.05 ± 0.42	0.144 ± 0.008	0.62 ± 0.20

[a]Values are daily arithmetical mean ± standard deviation. The "Back Trajectory" column indicates the direction and speed of advection for this day's air masses.

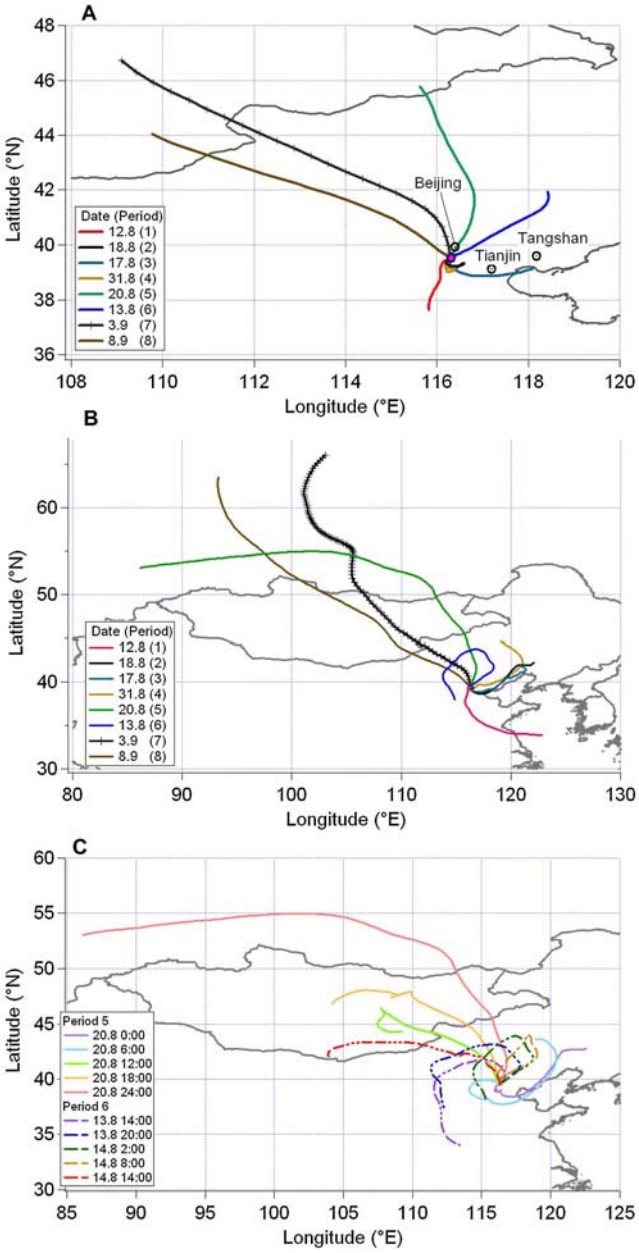

Figure 9. HYSPLIT (a) 24-h back trajectories and (b) 4-day back trajectories for all highlighted periods (start time 2400 LT of date indicated in legend); and (c) 4-day trajectories for Periods 5 and 6. All times refer to local time and all trajectories had an initial elevation of 100 m.

the north (e.g., Periods 5–8). When the air mass recently came from the south of Beijing, the $\sigma_{s,550}$, $\sigma_{a,532}$, Ångström and ω_{532} were generally higher and the b were generally lower than when the air mass originated in the north. These trends indicate that the southerly inflow to Beijing (i.e., when air masses recently came from the south and were measured at Yufa before flowing into and through Beijing) has a higher aerosol loading with "brighter" and on average smaller particles than the outflow from Beijing (i.e., when air masses were recently from the north and flowed through Beijing before arriving at the Yufa measurement site). The aerosol particles in the southerly flow also had a higher amount of sulfate and oxidized organic aerosol, suggesting a higher proportion of secondary aerosol (Takegawa et al., submitted manuscript, 2009).

[35] The larger Ångström exponents in the southerly inflow to Beijing indicate smaller average particle diameters, which appears to be driven by an increase in the fine/coarse ratio and not a decrease in modal diameter. In fact, using the Aerodyne Aerosol Mass Spectrometer, Takegawa et al. (submitted manuscript, 2009) found that the fine particle modal aerodynamic vacuum diameter increases steadily throughout these buildup periods [*Takegawa et al.*, 2009]. The aerosol size distribution data (D_p = 50 nm to 10 μm as described in section 2.1) for the highlighted periods confirm that the PM1/PM10 ratio indeed increases from ~30% to ~60% when the air masses originate in the north or south, respectively. The PM1 mass concentrations during the highlighted periods are on average seven times greater when the air mass originated in the south, while the coarse fraction mass (D_p = 1 − 10 μm) is only ~1.8 times larger with the southerly winds. These changes can also be seen in the AERONET data collected in this area. When the transition from southerly to northerly winds occurs the fine/coarse fraction decreases substantially owing mainly to a large decrease in the fine fraction and only a minimal decrease in the coarse fraction.

[36] The extensive properties and ω_{532} in the outflow of Beijing are consistent with a clean air mass that passes quickly over an area of increased combustion emissions (i.e., traffic emissions from Beijing). Interestingly, *Yan et al.* [2008], who measured ground-based aerosol optical properties ~100 km northeast of Beijing, also noted lower ω values when the air mass originated from the north, even though these air masses would not have traveled over urban Beijing. However, the range of ω values for northerly air masses (ω = 0.78–0.92) from *Yan et al.* [2008] was higher than in this current study (ω = 0.62–0.78), suggesting an approximate twofold increase in the proportion of absorbing particulate matter when the air mass travels over Beijing.

[37] Even days with similar 24-h back trajectories (i.e., both Period 5 and Period 7 have northerly 24-h back trajectories) have differences in their 24-h averaged optical properties, however. These differences were probed by analyzing the 4-day back trajectories (Figures 9b and 9c). The cleanest of the highlighted periods were Periods 7 and 8. As can be seen in Figure 9b, these air masses would not have encountered any large continental sources other than Beijing for the past 4 days, passing mostly over Mongolia. The 4-day back trajectories for Periods 2–4 are very similar, as are their intensive property averages in Table 2, though the extensive properties are not; these differences are most likely due to differences in aerosol loading and not in the intrinsic properties and sources of the particles. Periods 5 and 6 had 4-day back trajectories that changed during the day and include both northerly and circulating local trajectories (Figure 9c). Thus, as is evident in Table 2, these two periods can be considered an intermediate or mixed case as they had extensive and intensive properties that were in between the clean northerly and the more polluted southerly cases. However, even though the aerosol optical properties of the air masses for all the highlighted periods are influenced by their multiday back trajectories, they are primarily impacted by their 1-day history, with less, but more highly

Table 3. Comparison of Aerosol Optical Properties in the Northerly Outflow of Guangzhou/PRD During PRIDE-PRD2006 and in the Southerly Inflow and Outflow of Beijing During CAREBeijing-2006[a]

	PRIDE-PRD Average Outflow PRD	PRIDE-PRD Highly Polluted Outflow PRD	CAREBeijing Highly Polluted Inflow Beijing	PRIDE-PRD Less Polluted Outflow PRD	CAREBeijing Less Polluted Outflow Beijing
$\sigma_{s,450}$ (Mm^{-1})	200 ± 133	304 ± 139	528 ± 219	130 ± 49	36 ± 20
$\sigma_{bs,450}$ (Mm^{-1})	22.4 ± 13.7	35 ± 15	51 ± 18	15.6 ± 6	5 ± 3
$\sigma_{s,550}$ (Mm^{-1})	151 ± 103	226 ± 108	399 ± 174	96 ± 35	29 ± 17
$\sigma_{bs,550}$ (Mm^{-1})	18.0 ± 11.2	28 ± 12	42 ± 15	13 ± 4.7	4 ± 2
$\sigma_{s,700}$ (Mm^{-1})	104 ± 72	154 ± 78	268 ± 121	67 ± 24	37 ± 20
$\sigma_{bs,700}$ (Mm^{-1})	15.4 ± 9.7	23 ± 11	37 ± 14	11 ± 3.8	4 ± 2
$\sigma_{a,532}$ (Mm^{-1})	34.3 ± 26.5	47 ± 36	50 ± 21	28 ± 14	15 ± 8
$å_s$(550/700)	1.51 ± 0.22	1.60 ± 0.23	1.66 ± 0.12	1.47 ± 0.24	1.17 ± 0.20
$å_s$(450/700)	1.46 ± 0.21	1.54 ± 0.25	1.57 ± 0.15	1.46 ± 0.21	1.08 ± 0.35
$å_s$(450/550)	1.38 ± 0.22	1.46 ± 0.28	1.45 ± 0.19	1.44 ± 0.19	1.16 ± 0.18
b_{450}	0.116 ± 0.013	0.117 ± 0.015	0.101 ± 0.011	0.122 ± 0.012	0.135 ± 0.008
b_{550}	0.124 ± 0.015	0.126 ± 0.019	0.111 ± 0.016	0.133 ± 0.012	0.143 ± 0.007
b_{700}	0.154 ± 0.017	0.157 ± 0.020	0.145 ± 0.020	0.162 ± 0.013	0.165 ± 0.009
ω_{532}	0.82 ± 0.07	0.84 ± 0.06	0.89 ± 0.03	0.79 ± 0.06	0.65 ± 0.17

[a]Values are arithmetical mean values ± standard deviation. For PRIDE-PRD, highly polluted (10, 12, 20, and 21 July 2006) and less polluted (3, 4, 18, and 28 July 2006) mean that the measured air masses spent >24 or <24 h, respectively, over land. For CAREBeijing, highly polluted and less polluted are Periods 1–4 and Periods 7–8, respectively, from Table 2.

absorbing, particulate matter coming with the northerly winds.

[38] In summary, the relationship between air mass origin and aerosol optical properties indicates that the local particulate pollution in Beijing is dominated by a high proportion of light-absorbing material, most likely from diesel combustion and traffic emissions. The air masses that originate in the south carry a higher loading of particles with a higher scattering efficiency due to a higher amount of secondary aerosol components like sulfate and organics (Takegawa et al., submitted manuscript, 2009).

3.4. Comparisons to the Program of Regional Integrated Experiments of Air Quality Over the Pearl River Delta (PRIDE-PRD2006) Campaign

3.4.1. Extensive and Intensive Properties

[39] Immediately before the CAREBeijing-2006 campaign, the exact same instrumentation and setup was used in the PRIDE-PRD2006 campaign to measure the aerosol optical properties at a rural site (Backgarden) ~60 km northwest of the emerging megacity Guangzhou in the Pearl River Delta (PRD) [*Garland et al.*, 2008]. During that campaign, the air masses generally originated from the southeast, and passed over the very industrialized PRD region, which includes Hong Kong, Guangzhou and several other cities, before arriving at the Backgarden measurement site (monsoon circulation). Thus, the measurement data from the two campaigns allow for an insightful comparison of the particulate air pollution in two of the main city clusters of China during summer: outflow of Guangzhou/PRD during PRIDE-PRD2006 versus inflow and outflow of Beijing during CAREBeijing-2006.

[40] Table 3 shows the average aerosol optical properties observed during PRIDE-PRD2006 and during characteristic days when the air masses originated from the south/southeast. These days are categorized into ''Highly polluted'' periods when the air mass had spent >24 h over land (10, 12, 20 and 21 July 2006) and ''Less polluted'' periods when the air mass had spent <24 h over land (3, 4, 18 and 28 July 2006). Table 3 also displays the average optical parameters of characteristic days from CAREBeijing-2006 as highlighted in Table 2 and Figure 9, using the 24-h back-trajectory information to label ''Inflow'' (Periods 1–4) and ''Outflow'' (Periods 7 and 8).

[41] The campaign averages for σ_s in PRIDE-PRD2006 are approximately a factor of 2.4 smaller than the campaign averages for CAREBeijing-2006 ($\sigma_{s,550}$ = 151 ± 103 Mm^{-1} versus $\sigma_{s,550}$ = 361 ± 295 Mm^{-1}; Tables 1 and 3). Even during the ''Highly polluted'' days of PRIDE-PRD2006, the scattering coefficients in the outflow of Guangzhou/PRD were a factor of ~1.6 smaller than the CAREBeijing-2006 campaign average and a factor of ~2 smaller than the ''Highly polluted'' inflow into Beijing, indicating that in the summer, the particulate pollution in and around Beijing is substantially more extreme than in the PRD region.

[42] The campaign average of $\sigma_{a,532}$ was 1.5 times lower during PRIDE-PRD2006 ($\sigma_{a,532}$ = 34.3 ± 26.5 Mm^{-1}) than during CAREBeijing-2006 ($\sigma_{a,532}$ = 51.8 ± 36.5 Mm^{-1}). During the ''Highly polluted'' periods, however, the absorption coefficients were similarly high near Guangzhou ($\sigma_{a,532}$ = 47 ± 36 Mm^{-1}) and near Beijing ($\sigma_{a,532}$ = 50 ± 21 Mm^{-1}). Thus, on average, as well as during the ''Highly polluted'' periods for both campaigns, the inflow into Beijing had substantially larger scattering coefficients and higher single scattering albedos than the outflow of Guangzhou/PRD.

[43] Comparing the ''Less polluted'' periods when relatively clean and fast moving air masses passed over the urban areas before being sampled at the measurement sites, the scattering and absorption coefficients were by factors of 2–3 higher in the outflow of Guangzhou/PRD ($\sigma_{s,550}$ = 96 ± 35 Mm^{-1}, $\sigma_{a,532}$ = 28 ± 14 Mm^{-1}) than in the outflow of Beijing ($\sigma_{s,550}$ = 29 ± 17 Mm^{-1}, $\sigma_{a,532}$ = 15 ± 8 Mm^{-1}). During the less polluted periods, the single scattering albedos were lower than the averages of both campaigns, but the difference was more pronounced for the outflow of Beijing (ω_{532} = 0.65 ± 0.17 versus 0.86 ± 0.07) than for the outflow of Guangzhou/PRD (ω_{532} = 0.79 ± 0.06 versus 0.82 ± 0.07). These results indicate that combustion sources of light absorbing carbon, such as diesel soot from traffic emissions, are strong in both megacities but more dominant in Beijing.

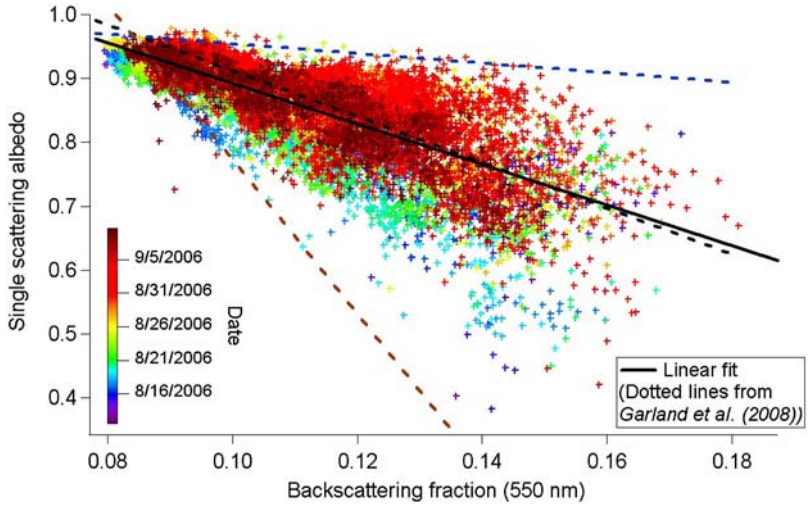

Figure 10. Single scattering albedo (ω_{532}) versus backscattering fraction at $\lambda = 550$ nm (b_{550}). The solid black line is a linear best fit through the data points, which are color-coded by date. The dotted lines are the best fit (black dotted line) and boundary conditions (brown and blue dotted lines) for the ω_{532} versus b_{550} relationship in PRIDE-PRD2006 campaign [*Garland et al.*, 2008].

[44] The Angstrom exponents were generally similar for both campaigns (1.4 to 1.7), but much lower in the outflow of Beijing during the "Less polluted" periods (1.1 to 1.2). As described above, these low $\mathring{a}_s$ values can be attributed to an increase in the relative proportion of the coarse particle fraction.

3.4.2. Radiative Forcing Sensitivities

[45] As detailed by *Garland et al.* [2008], a negative correlation between ω_{532} and b_{550} was observed during PRIDE-PRD2006. Using the radiative forcing equation from *Haywood and Shine* [1995] a sensitivity study of the radiative forcing efficiency ($\Delta F/\delta$; defined as the forcing per unit aerosol optical depth) was performed. The coupling of ω_{532} and b_{550} was found to have a strong impact on $\Delta F/\delta$, with a tendency to decrease the cooling potential of the particles. For a full discussion of sensitivities and implications see *Garland et al.* [2008], who, to our knowledge, provided the first study addressing this issue.

[46] During CAREBeijing-2006 we observed a similar inverse relationship between ω_{532} and b_{550} as during PRIDE-PRD2006. Figure 10 displays ω_{532} versus b_{550} with a linear fit to the data. Additionally, the dotted lines represent the linear fit (black dotted line) and boundary conditions (red and blue dotted lines) for the PRIDE-PRD2006 campaign [*Garland et al.*, 2008]. The linear fits for both of these campaigns are very similar, and the boundary conditions for PRIDE-PRD2006 capture most of the CAREBeijing-2006 data. Thus, similar implications can be expected and the observed coupling of ω_{532} and b_{550} should be considered when modeling the radiative forcing of aerosols in these regions.

4. Summary and Conclusions

[47] Aerosol optical properties were measured at a suburban site south of Beijing as part of CAREBeijing-2006 field campaign, during the similar time period when the Summer Olympics would be held in 2008. The extensive properties (σ_s and σ_a) and ω_{532} at this suburban site were similar to other measurements in Chinese urban and suburban areas.

[48] Pronounced diurnal cycles were observed for ω_{532}, σ_s and σ_a. The σ_s and σ_a values had their maxima during the late evening–early morning as the nocturnal boundary layer formed while surface emissions continued, and then decreased during the day owing to mixing with the overlying residual layer. Additionally, the σ_a cycle had a peak at dawn that was not present in the σ_s cycle and may be due to local diesel emissions; this enhancement also impacts the ω_{532} diurnal cycle that had a minimum at sunrise. Thus, these diurnal cycles are controlled by a combination of mixing due to the formation and breakup of a nocturnal boundary layer together with an enhancement of absorbing particles around sunrise.

[49] The meteorology was a key factor in controlling the aerosol optical properties. Eight periods of the campaign were highlighted to examine the impact of air mass origin on the aerosol optical properties. Both the extensive and the intensive properties were highly dependent upon the origin of the air mass. This indicates that not only does the aerosol concentration change with air mass origin, but so do the chemical composition and sources. When the measured air masses originated in the north and passed over Beijing, the single scattering albedo was generally low (<0.8), which indicates that the local emissions of air particulate matter in Beijing were dominated by primary particles from combustion sources (e.g., diesel soot from traffic). The southerly inflow to Beijing had typically very high absorption and scattering coefficients (i.e., very high aerosol concentration) and higher than average single scattering albedo and Ångström exponents, suggesting a large proportion of small particles and secondary chemical components (e.g., sulfates and oxidized organics). The size distribution data (from both TDMPS + APS in situ measurements and AERONET retrievals) also showed an increase in the total PM10 mass concentration when the winds changed from north to south, whereby the increase in PM1 was ~4 times greater than the

increase of the coarse fraction (PM10-PM1) and this may drive the dependence of the Ångström exponent on wind direction and air mass origin.

[50] Identical instrumentation was used in the PRIDE-PRD2006 campaign (1–30 July 2006) in a rural site outside of Guangzhou that was held directly before the CARE-Beijing-2006 campaign. In the PRIDE-PRD2006 campaign, the outflow of the heavily industrialized and populated Pearl River Delta Region was measured during the rainy season. The scattering and absorption coefficients measured in the outflow of the Pearl River Delta Region were ~2 times smaller than the southerly inflow into Beijing. Overall, the results suggest that the inflow of regional pollution from the south of Beijing is substantial and greatly impacts the amount and characteristics of the particulate pollution in urban Beijing.

[51] **Acknowledgments.** The CAREBeijing-2006 (Campaign of Air Quality Research in Beijing and surrounding areas in 2006) was supported by the Beijing Council of Science and Technology (HB200504-6, HB200504-2). This study was supported by the Max Planck Society (MPG), the Leibniz Institute for Tropospheric Research (IfT), the University of Tokyo (UT) and Peking University (PKU). Thanks go to RCEC (Research Center for Environmental Changes, Academic Sinica) for providing the AERONET data, Guo Song for the average meteorological values, and Chen Chen-Yong for the population density map. The authors gratefully acknowledge the NOAA Air Resources Laboratory (ARL) for the provision of the HYSPLIT transport and dispersion model and/or READY website (http://www.arl.noaa.gov/ready.html) used in this publication. Thanks are owed to all team members for support during the campaign and fruitful discussions afterward.

References

Anderson, T. L., and J. A. Ogren (1998), Determining aerosol radiative properties using the TSI 3563 integrating nephelometer, *Aerosol Sci. Technol.*, *29*, 57–69, doi:10.1080/02786829808965551.

Anderson, T. L., et al. (1996), Performance characteristics of a high-sensitivity, three-wavelength, total scatter/backscatter nephelometer, *J. Atmos. Oceanic Technol.*, *13*, 967–986, doi:10.1175/1520-0426(1996)013<0967:PCOAHS>2.0.CO;2.

Andreae, M. O., et al. (2008), Optical properties and chemical composition of the atmospheric aerosol in urban Guangzhou, China, *Atmos. Environ.*, *42*, 6335–6350, doi:10.1016/j.atmosenv.2008.01.030.

Ångström, A. (1929), On the atmospheric transmission of sun radiation and on dust in the air, *Geogr. Ann.*, *11*, 156–166, doi:10.2307/519399.

Arnott, W. P., et al. (1999), Photoacoustic spectrometer for measuring light absorption by aerosol: Instrument description, *Atmos. Environ.*, *33*, 2845–2852, doi:10.1016/S1352-2310(98)00361-6.

Arnott, W. P., et al. (2000), Nitrogen dioxide and kerosene-flame soot calibration of photoacoustic instruments for measurement of light absorption by aerosols, *Rev. Sci. Instrum.*, *71*, 4545–4552, doi:10.1063/1.1322585.

Bergin, M. H., et al. (2001), Aerosol radiative, physical, and chemical properties in Beijing during June 1999, *J. Geophys. Res.*, *106*, 17,969–17,980, doi:10.1029/2001JD900073.

Chan, C. K., and X. Yao (2008), Air pollution in mega cities in China, *Atmos. Environ.*, *42*, 1–42, doi:10.1016/j.atmosenv.2007.09.003.

Chen, D. S., et al. (2007), An integrated MM5-CMAQ modeling approach for assessing trans-boundary PM10 contribution to the host city of 2008 Olympic summer games—Beijing, China, *Atmos. Environ.*, *41*, 1237–1250, doi:10.1016/j.atmosenv.2006.09.045.

Cheng, Y. F., et al. (2009), Aerosol optical properties and related chemical apportionment at Xinken in Pearl River Delta of China, *Atmos. Environ.*, doi:10.1016/j.atmosenv.2008.02.034, in press.

Garland, R., et al. (2008), Aerosol optical properties in a rural environment near the mega-city Guangzhou, China: Implications for regional air pollution, radiative forcing and remote sensing, *Atmos. Chem. Phys.*, *8*, 5161–5186.

Haywood, J. M., and K. P. Shine (1995), The effect of anthropogenic sulfate and soot aerosol on the clear-sky planetary radiation budget, *Geophys. Res. Lett.*, *22*, 603–606, doi:10.1029/95GL00075.

Keeling, R. F., et al. (1996), Global and hemispheric CO_2 sinks deduced from changes in atmospheric O_2 concentration, *Nature*, *381*, 218–221, doi:10.1038/381218a0.

Li, C., L. T. Marufu, R. R. Dickerson, Z. Li, T. Wen, Y. Wang, P. Wang, H. Chen, and J. W. Stehr (2007a), In situ measurements of trace gases and aerosol optical properties at a rural site in northern China during East Asian Study of Tropospheric Aerosols: An International Regional Experiment 2005, *J. Geophys. Res.*, *112*, D22S04, doi:10.1029/2006JD007592.

Li, Y., et al. (1993), Use of 2nd derivatives of canopy reflectance for monitoring prairie vegetation over different soil backgrounds, *Remote Sens. Environ.*, *44*, 81–87, doi:10.1016/0034-4257(93)90104-6.

Li, Z. Q., et al. (2007b), Aerosol optical properties and their radiative effects in northern China, *J. Geophys. Res.*, *112*, D22S01, doi:10.1029/2006JD007382.

Schmid, O., et al. (2006), Spectral light absorption by ambient aerosols influenced by biomass burning in the Amazon Basin. I: Comparison and field calibration of absorption measurement techniques, *Atmos. Chem. Phys.*, *6*, 3443–3462.

Schnaiter, M. (2005), Measurement of wavelength-resolved light absorption by aerosols utilizing a UV-VIS extinction cell, *Aerosol Sci. Technol.*, *39*, 249–260.

Shao, M., et al. (2006), City clusters in China: Air and surface water pollution, *Frontiers Ecol. Environ.*, *4*, 353–361, doi:10.1890/1540-9295(2006)004[0353:CCICAA]2.0.CO;2.

Streets, D. G., et al. (2007), Air quality during the 2008 Beijing Olympic Games, *Atmos. Environ.*, *41*, 480–492, doi:10.1016/j.atmosenv.2006.08.046.

Takegawa, N., T. Miyakawa, Y. Kondo, J. L. Jimenez, Q. Zhang, D. R. Worsnop, and M. Fukuda (2006), Seasonal and diurnal variations of submicron organic aerosol in Tokyo observed using the Aerodyne aerosol mass spectrometer, *J. Geophys. Res.*, *111*, D11206, doi:10.1029/2005JD006515.

Takegawa, N., et al. (2009), Performance of an aerodyne aerosol mass spectrometer (AMS) during intensive campaigns in China in the summer of 2006, *Aerosol. Sci. Technol.*, in press.

Wehner, B., et al. (2008), Relationships between submicrometer particulate air pollution and air mass history in Beijing, China, 2004–2006, *Atmos. Chem. Phys.*, *8*, 6155–6168.

Xia, X. A., et al. (2005), Aerosol properties and their spatial and temporal variations over North China in spring 2001, *Tellus, Ser. B*, *57*, 28–39, doi:10.1111/j.1600-0889.2005.00126.x.

Xia, X. A., H. B. Chen, P. C. Wang, W. X. Zhang, P. Goloub, B. Chatenet, T. F. Eck, and B. N. Holben (2006), Variation of column-integrated aerosol properties in a Chinese urban region, *J. Geophys. Res.*, *111*, D05204, doi:10.1029/2005JD006203.

Xia, X., H. Chen, P. Goloub, W. Zhang, B. Chatenet, and P. Wang (2007a), A compilation of aerosol optical properties and calculation of direct radiative forcing over an urban region in northern China, *J. Geophys. Res.*, *112*, D12203, doi:10.1029/2006JD008119.

Xia, X., et al. (2007b), Analysis of the dependence of column-integrated aerosol properties on long-range transport of air masses in Beijing, *Atmos. Environ.*, *41*, 7739–7750, doi:10.1016/j.atmosenv.2007.06.042.

Xu, J., et al. (2002), Measurement of aerosol chemical, physical and radiative properties in the Yangtze delta region of China, *Atmos. Environ.*, *36*, 161–173, doi:10.1016/S1352-2310(01)00455-1.

Yan, P., et al. (2008), The measurement of aerosol optical properties at a rural site in Northern China, *Atmos. Chem. Phys.*, *7*, 2229–2242.

P. Achtert, A. Nowak, and A. Wiedensohler, Leibniz Institute for Tropospheric Research, Permoserstrasse 15, D-04318 Leipzig, Germany. (achtert@mail.tropos.de; nowak@tropos.de; ali@tropos.de)

M. O. Andreae, R. M. Garland, S. S. Gunthe, and U. Pöschl, Biogeochemistry Department, Max Planck Institute for Chemistry, Becherweg 27, D-55128 Mainz, Germany. (andreae@mpch-mainz.mpg.de; garland@mpch-mainz.mpg.de; gunthe@mpch-mainz.mpg.de; poeschl@mpch-mainz.mpg.de)

M. Hu, M. Shao, L. M. Zeng, and T. Zhu, State Key Joint Laboratory of Environmental Simulation and Pollution Control, College of Environmental Sciences and Engineering, Peking University, Beijing 100871, China. (minhu@pku.edu.cn; mshao@pku.edu.cn; lmzeng@pku.edu.cn; tzhu@pku.edu.cn)

K. Kita, College of Science, Ibaraki University 2-1-1 Bunkyo, Mito 310-8512, Japan. (kita@mx.ibaraki.ac.jp)

Y. Kondo and N. Takegawa, RCAST, University of Tokyo, 4-6-1 Komaba, Meguro-ku, Tokyo 153-8904, Japan. (kondo@atmos.rcast.u-tokyo.ac.jp; takegawa@atmos.rcast.u-tokyo.ac.jp)

O. Schmid, Institute for Inhalation Biology, German Research Center for Environmental Health, Helmholtz Center Munich, Ingolstadter Landstrasse 1, D-85764 Neuherberg, Germany. (otmar.schmid@fsf.de)